# Dynamic Fracture Toughness of Homalite-100

Dynamic fracture toughness of Homalite-100 determined by T. Kobayashi and Dally, as well as those of Araldite B by Kalthoff, Beinert and Winkler, are compared with those of the authors' previous results. Errors generated through the use of static near-field crack-tip stresses for evaluating dynamic stress-intensity factor are also discussed

by A.S. Kobayashi and S. Mall

ABSTRACT—Dynamic fracture toughness of Homalite-100 determined by T. Kobayashi and Dally are compared with those previously obtained by the authors where similarities in the two results for single-edged-notch specimens of various configurations are noted. Dynamic fracture toughness of Araldite B obtained by Kalthoff, Beinert and Winkler and those of Homalite-100 obtained by the authors are then compared and, again, similarities in the two results and, in particular, the scatters in experimental data for wedge-loaded DCB specimens of different sizes are found. All three teams of investigators used static near-field solution to compute the dynamic stress-intensity factors from recorded dynamic isochromatics or dynamic caustics. Errors generated through this use of static near-field solutions, as well as through the use of larger isochromatic lobes, are thus discussed.

## Introduction

For the past several years, the writers and their colleagues have been using dynamic photoelasticity to determine the dynamic stress-intensity factors* and crack velocities of propagating cracks in unstiffened and stiffened single-edged-notch (SEN) tension plates under fixed grip loading, with and without impact conditions,[1,2] dynamic-tear-test (DTT) specimens,[3] and wedge-loaded double-cantilever-beam (DCB) specimens.[4] In all these studies, a static near-field solution was used to compute the dynamic stress-intensity factor from the dynamic isochromatic patterns surrounding the running crack following Irwin's procedure of 1958.[5] More recently, T. Kobayashi and Dally have used dynamic photoelasticity to determine dynamic fracture toughness of propagating cracks in various birefringent polymers.[6,7] Also Kalthoff *et al.* have, through the use of caustics, determined the dynamic fracture toughness of Araldite B using wedge-loaded DCB specimens.[8] The results obtained by these three independent teams of researchers, at first, appeared to be mutually contradictory to the extent that some results are quoted out of context to support a particular fracture-dynamic and crack-arrest criteria against others. The purpose of this paper is to identify some of the common results obtained among these three teams of investigators and to analyze the possible causes which led to these apparent discrepancies.

## Dynamic Fracture Toughness

In the three investigations quoted above, a static near-field state of stress was fitted to either the dynamic isochromatics or the dynamic caustics surrounding a running crack, and the static stress-intensity factor thus obtained was considered to be the dynamic stress-intensity factor. Ignoring for the time being the inherent, as well as additional, possible sources of errors involved in this data-reduction scheme, the dynamic stress-intensity factor, as defined by the static near-field solution, vs. crack-velocity relation can be plotted in a nondimensional format in order to reduce as much as possible the effects of material variabilities between the three investigators. Figure 1 shows the nondimensionalized crack velocity vs. nondimensionalized dynamic-fracture-toughness relation obtained from the dynamic photoelastic data in Homalite-100 plate, 9.5 mm (3/8 in.) in thickness, by Bradley[1] who used 254 mm × 254 mm (10 in. × 10 in.) single-edged-notch plates under fixed-grip condition. Most of the data scatter in Fig. 1 is mainly due to inaccurate crack-velocity measurements which were calculated directly from the crack-tip position vs. time data and is also due in part to the stress-wave effects. T. Kobayashi and Dally,[7] on the other hand, used smoothed crack-tip position vs. time curves for crack-velocity calculations and observed no stress-wave effects. The uniform crack velocity thus

*A.S. Kobayashi and S. Mall are Professor and Postdoctoral Research Associate, respectively, Department of Mechanical Engineering, University of Washington, Seattle, WA 98195.*

*Paper was presented at 1977 SESA Spring Meeting held in Dallas, TX on May 15-20.*

*Original manuscript submitted: January 12, 1977. Final version received: May 28, 1977.*

* *Dynamic stress-intensity factor of a running crack in a particular material is referred to as dynamic fracture toughness or the dynamic fracture resistance, $K_{ID}$, of the material.*

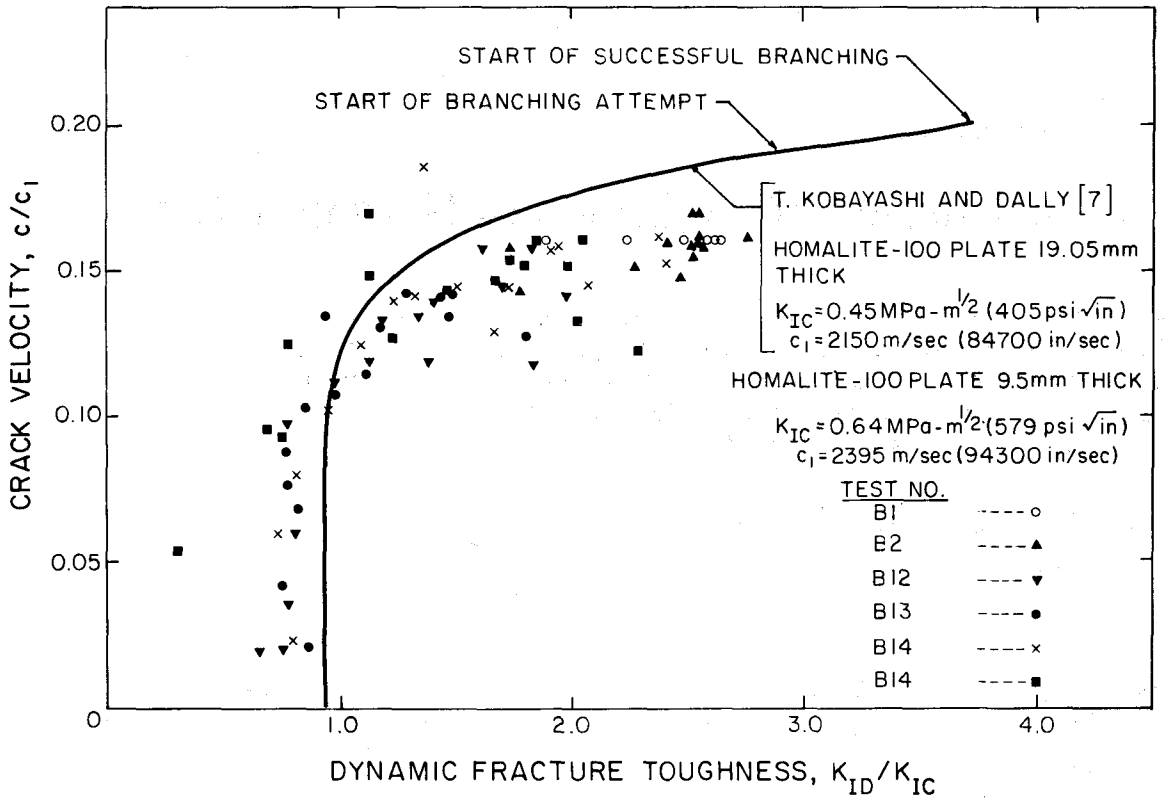


Fig. 1—Crack-velocity vs. Dynamic-fracture-toughness relations of single-edged-notch Homalite-100 plates

obtained from the smoothed-crack length vs. time curve is consistent with the uniform crack velocities observed in fracturing glass using ultrasonic-ripple marking technique[9] and in polymethylmethacrylate using streak photography.[10] By compressing our scatters in crack velocities, we too can obtain a better correlation between dynamic stress-intensity factor and crack velocity as shown in Fig. 2.

The dynamic-fracture-toughness vs. crack-velocity relation by T. Kobayashi and Dally[7] for 19.05-mm-thick Homalite-100 plates was converted to nondimensionalized-dynamic-fracture-toughness vs. nondimensionalized-crack-velocity relation and is also plotted in Figs. 1 and 2. Despite the scatter in our data, the two nondimensionalized dynamic fracture toughnesses at the lower crack velocities agree well, particularly when one considers the differences in the material properties of the Homalite-100 plates of different thicknesses and of different fabrication periods. The static fracture toughnesses of the two different Homalite-100 plates differed by approximately 30 percent and the estimated differences between the nondimensionalized averaged dynamic stress-intensity factor at crack arrest was about 12 percent. These differences could be partly attributed to our overestimated static fracture toughness which was determined from SEN tension specimen with sawed and chiseled crack instead of the fatigued crack used by T. Kobayashi and Dally.[7]

Although one can construct an averaged dynamic-fracture-toughness vs. crack-velocity relation which assumes the familiar Γ-shaped curve,[11] through the scattered experimental data in Fig. 2, we are reluctant to establish such definitive dynamic-fracture characterization in view of our recent experiences with dynamic-finite-element analysis of a fracturing tapered DCB specimen[12] and dynamic-finite-difference analyses of fracturing pipes.[13] The results of these numerical analyses indicate that an elastic crack must run at intermittent crack velocities in order for a smoothly varying dynamic-fracture-toughness vs. crack-velocity relation to exist as a material property. Alternatively, the dynamic fracture toughness must vary intermittently in order to maintain smoothly varying crack velocities and, thus, precludes a unique Γ-shaped crack-velocity vs. dynamic-stress-intensity-factor relation. At the present stage of development, in the writers' opinion, neither dynamic photoelasticity nor dynamic caustics can provide accurate dynamic stress-intensity factor nor crack velocity to resolve this controversy. In fact, the available little data on relatively accurate crack-velocity measurements indicate that the crack velocity does vary uniformly at least in glass[9] and in polymethylmethacrylate,[10] thus leaving us with the only alternatives of nonunique relation between dynamic stress-intensity factor and crack velocity if the above mentioned numerical analyses had correctly modeled dynamic fracture.

Figure 2 also shows another point of departure between our results and those of T. Kobayashi *et al.* who observed complete crack branching at $K_{ID}/K_{IC} = 3.7$,[7] where we could not relate crack branching with any instantaneous dynamic stress-intensity factor. Perhaps this difference in crack-branching dynamic fracture toughness also involves the definition of crack branching. Our fractured Homalite-100 specimens showed many minute crack branches prior to the onset of major crack branching as shown in Fig. 3.* Obviously considerable unaccountable fracture energy was

* *Figure 3 is an enlargement of Frame 13 in Fig. 2 of Ref. 14.*

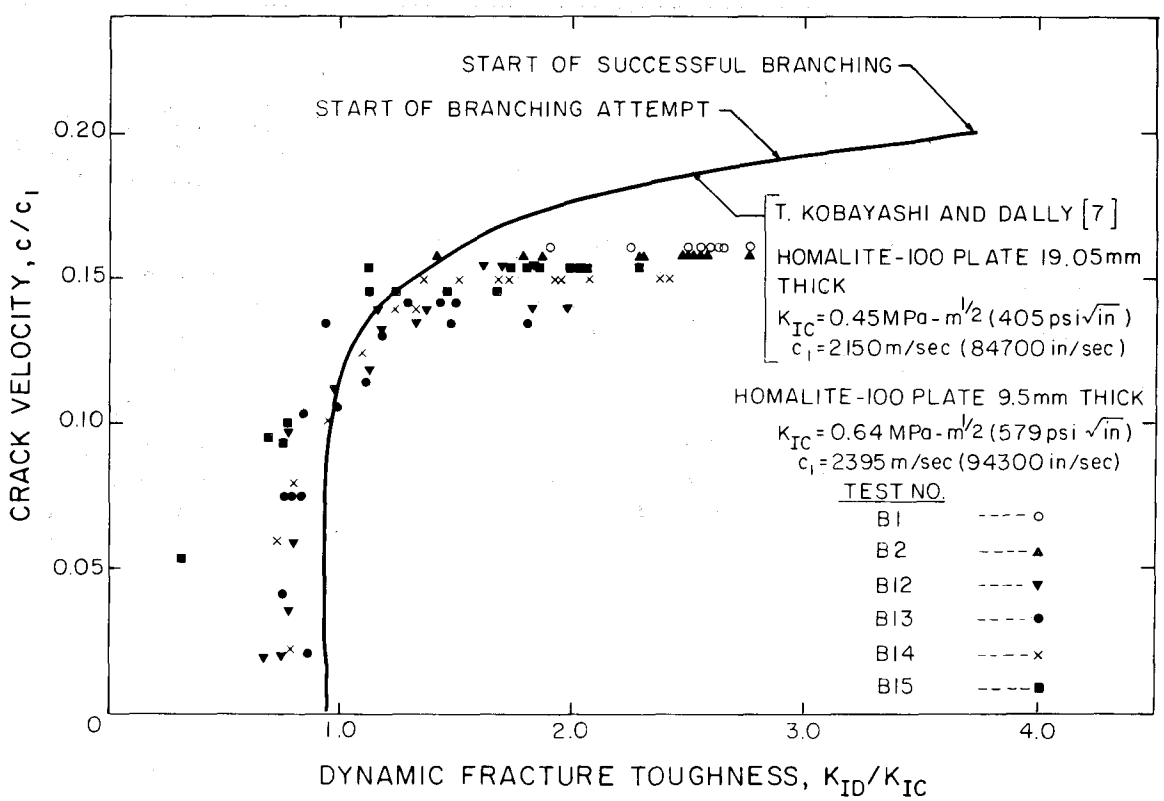


Fig. 2—Smoothed-crack-velocity vs. dynamic-fracture-toughness relations of single-edged-notch Homalite-100 plates

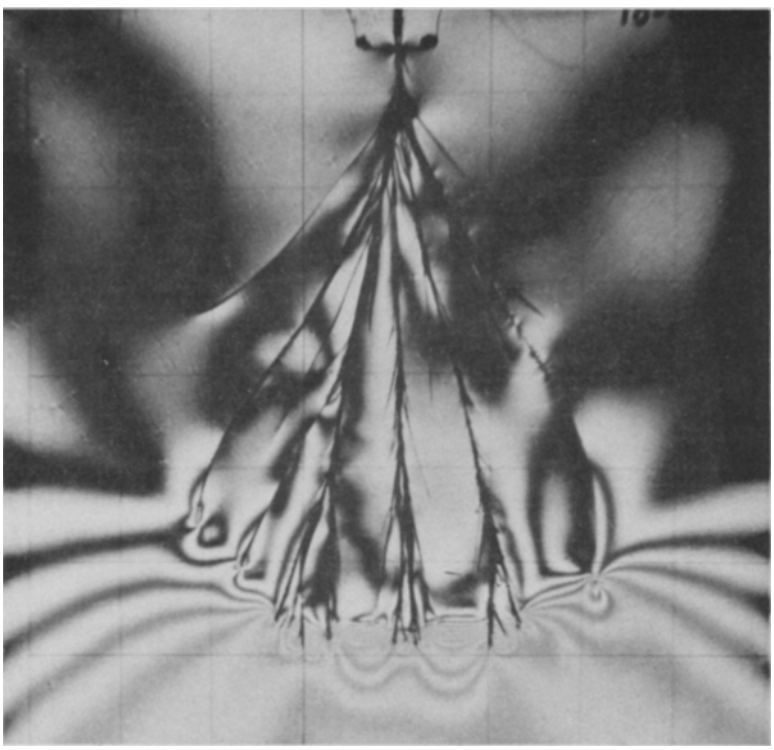

Fig. 3—Crack branching in Homalite-100 plate[4]

dissipated through these minor crack branches which could have resulted in our indecisive crack-branching dynamic fracture toughness. In addition, the close proximity of the two running cracks, which just branched,

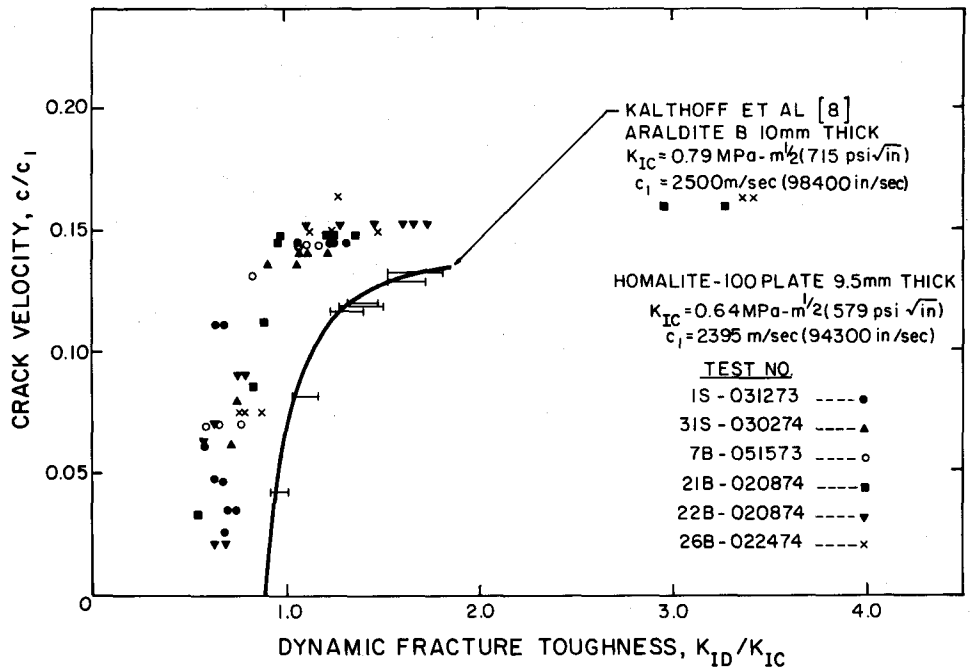


Fig. 4—Smoothed-crack-velocity vs. dynamic-fracture-toughness relations of wedge-loaded DCB specimens

accentuates the interchange between the dynamic energy released and the kinetic energy surrounding the crack tip.[15] Thus the static near-field solution can no longer be used for calculating the dynamic stress-intensity factor of a bifurcated or trifurcated crack surrounded by a single dynamic isochromatic lobe. Lacking a proper data-reduction procedure, a gross energetic approach was used to arrive at an empirical crack-branching criterion.

As for a crack-branching criterion based on energetics, an average dynamic energy-release rate, which is defined as the total dynamic energy released divided by the total crack surface, was computed by using the single-crack-tip near-field solution, but by incorporating all measurable major and minor crack surfaces. This average dynamic energy-release rate, $G_{ID}]_{ave}$, which incorporates the gross effect of kinetic-energy feedback for driving the crack, was found to be of 2.1 - 2.7 times the static critical strain-energy-release rate, $G_{IC}$.[14] This crudely estimated crack branching $G_{ID}]_{ave}$ indicates that branching will occur when sufficient energy is available to propagate two separate cracks. Obviously, further refinements of such data-reduction procedure are necessary before a crack branching criterion can be established. Our preference for using the dynamic energy-release rate instead of the more directly calculable dynamic stress-intensity factor from the dynamic isochromatics and dynamic caustic as per T. Kobayashi *et al.*,[7] and Kalthoff *et al.*,[8] respectively, is attributed to the fact that the sum of dynamic energy-release rate during crack propagation can be related to the total kinetic energy and potential energy in the test specimen under fixed grip loading at each instant of time, thus providing an accuracy assessment based on first principles. Computation of this dynamic energy released, $G_{ID}$, from dynamic fracture toughness, $K_{ID}$, was accomplished by Freund's formula[16] using the measured crack velocity. The generality of this part of Freund's solution was discussed by Nilsson.[17]

Figure 4 shows a comparison between the dynamic fracture toughness vs. smoothed-crack velocities in wedge-loaded DCB specimens of Araldite B[8] and Homalite-100.[4] Here, again, the smoothed-crack length-vs.-time curve was used to eliminate the many oscillations in crack velocities, thus making it similar in shape to Kalthoff's curve. Although no direct correlation between the two 'Γ' curves is possible due to differences in material properties between Araldite B and Homalite-100, it is interesting to note that scatters, which were appreciably larger than those of T. Kobayashi *et al.*, in data points of these two materials are very similar in these nondimensionalized plots. This scatter could be due to the larger interaction between kinetic energy and dynamic energy released in our smaller DCB specimens in contrast to the large monolithic single-edged notch specimens used by T. Kobayashi and Dally. An up-to-date detailed discussion on the high dynamic amplification factor due to this intense interchange between kinetic energy and dynamic energy released through crack propagation in wedge-loaded DCB specimen can be found in Ref. 18.

It is interesting to note that in Kalthoff's experiment, the dynamic stress-intensity factor oscillated after crack arrest, eventually converging to the static stress-intensity factor at crack arrest, $K_{Ia}$, which gradually decreased with increasing arrest-crack length. This gradual decrease in $K_{Ia}$ with higher driving force of $K_{IQ}$ is in accord with the belief that the static stress-intensity factor at crack arrest is not a material property.[8,15,18,19]

The above comparison of experimental results shows that, although the results obtained by the three teams are in qualitative agreement with each other, data scatter in Kalthoff's and our experiments were consistently larger than those of T. Kobayashi and Dally. It thus appeared appropriate to reassess our data-reduction scheme at this time in search of the cause or causes of the data scatter in Kalthoff's and our results. As mentioned previously, the static near-field solution was used by all to reduce their dynamic optical data. Kalthoff *et al.* and we used the optical data within a radial distance of $r = 2.5 \sim 5$-mm (0.1 ~ 0.2-in.) region surrounding the moving crack tip while T. Kobayashi *et al.*, in some of their data-reduction schemes, considered regions as large as $r \fallingdotseq 25.4$ mm (1

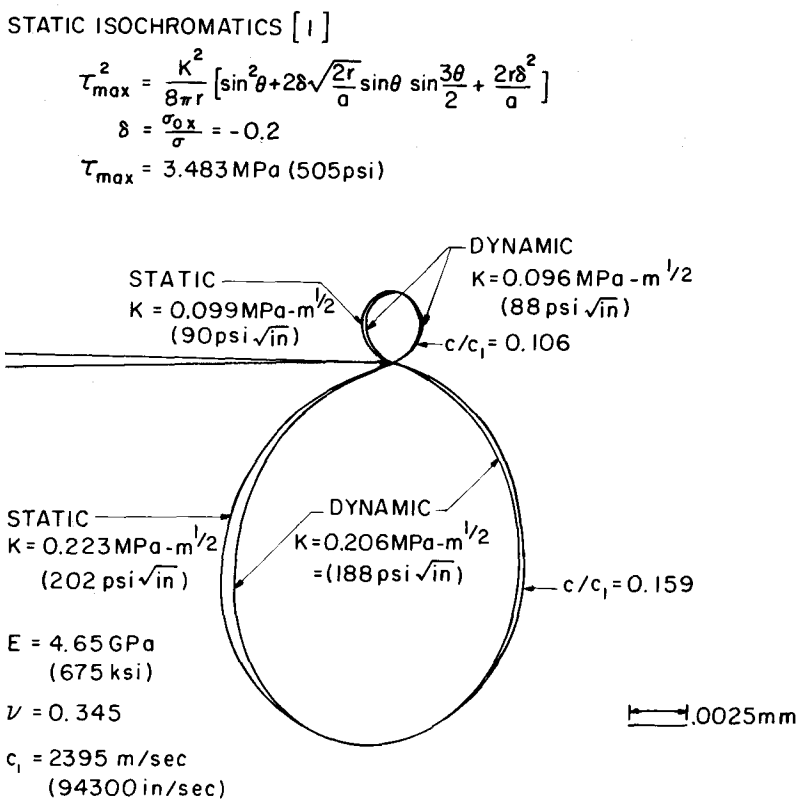


Fig. 5—Dynamic and static isochromatic lobes at the crack tip for constant $\tau_{max}$

in.).[20] The possible numerical errors involved in using larger crack-tip region in a uniform dynamic stress field surrounding a Yoffe crack[21] were discussed previously.[19] Since this error analysis did not incorporate the effect of nonuniform dynamic stress field, such error analysis is considered in the following section.

## Near-field Elasto-dynamic State

The near-field elasto-dynamic state of stresses for a crack propagating at a constant velocity, $c$, is[22]

$$\sigma_{xx} = a_1\frac{3}{2}\left\{(2s_1^2 - s_2^2 + 1)r_1^{-1/2}\cos\frac{\theta_1}{2} - \frac{4s_1s_2}{(1+s_2^2)}r_2^{-1/2}\cos\frac{\theta_2}{2}\right\} + a_2\,8(s_1^2 - s_2^2) + a_3\frac{15}{2}\left\{(2s_1^2 - s_2^2 + 1)\,r_1^{1/2}\cos\frac{\theta_1}{2} - \frac{4s_1s_2}{(1+s_2^2)}r_2^{1/2}\cos\frac{\theta_2}{2}\right\} + \ldots \quad (1a)$$

$$\sigma_{yy} = a_1\frac{3}{2}\left\{-(1+s_2^2)r_1^{-1/2}\cos\frac{\theta_1}{2} + \frac{4s_1s_2}{(1+s_2^2)}r_2^{-1/2}\cos\frac{\theta_2}{2}\right\} + a_3\frac{15}{2}\left\{-(1+s_2^2)r_1^{1/2}\cos\frac{\theta_1}{2} + \frac{4s_1s_2}{(1+s_2^2)}r_2^{1/2}\cos\frac{\theta_2}{2}\right\} + \ldots \quad (1b)$$

$$\tau_{xy} = a_1 3s_1\left\{r_1^{-1/2}\sin\frac{\theta_1}{2} - r_2^{-1/2}\sin\frac{\theta_2}{2}\right\} + a_3 15s_1\left\{-r_1^{1/2}\sin\frac{\theta_1}{2} + r_2^{1/2}\sin\frac{\theta_2}{2}\right\} + \ldots \quad (1c)$$

where

$$s_1^2 = 1 - c^2/c_1^2 \quad \text{and} \quad s_2^2 = 1 - c^2/c_2^2 \quad (2a)$$

$$r_1^2 = x^2 + s_1^2y^2 \quad \text{and} \quad r_2^2 = x^2 + s_2^2y^2 \quad (2b)$$

$$\tan\theta_1 = \frac{s_1y}{x} \quad \text{and} \quad \tan\theta_2 = \frac{s_2y}{x} \quad (2c)$$

$c$, $c_1$ and $c_2$ are the crack velocity, dilatational-wave velocity and distortional-wave velocity, respectively.
$x$ and $y$ are moving rectangular coordinates with origins at the propagating crack tip.

The above near-field state represents the first three terms in Ref. 22 and was selected for comparison with the three parameter representations in Ref. 20. It can be easily shown that for zero crack velocity or $c \to 0$, eqs (1) reduce to those in Ref. 23. The arbitrary constant coefficient, $a_1$, can also be represented in terms of the more familiar dynamic stress-intensity factor as

$$a_1 = \frac{K}{2\sqrt{2\pi}}\frac{4(1+s_2^2)}{3[4s_1s_2 - (1+s_2^2)^2]} \quad (3)$$

where $K$ is the dynamic stress-intensity factor after Freund[16] and reduces to the static stress-intensity factor when $c \to 0$. It can also be shown that $a_2 \to -\sigma_{ox}/[8(s_1^2 - s_2^2)]$ when $c \to 0$ where $\sigma_{ox}$ is the often-quoted remote-stress component.[5,7]

The dynamic isochromatic-fringe loop can be represented

by the well-known formula of

$$\tau_{max} = [(\sigma_{xx} - \sigma_{yy})^2/4 + \tau_{xy}^2]^{1/2} \quad (4)$$

The displacement, $\overline{w}$, of the constrained zone surrounding the crack tip in the method of caustics is[24]

$$\overline{w} = - z_o t f \text{ grad } (\sigma_{xx} + \sigma_{yy}) \quad (5)$$

where $z_o$, $t$ and $f$ are the distance between the midplane of the specimen and screen, thickness of the specimen and the optic constant of the specimen, respectively. In the following, eqs (1) and (4) will be used to establish the theoretical dynamic isochromatics for a known dynamic stress-intensity factor which will be compared with the stress-intensity factor computed by using the static near-field solutions.

## Dynamic Isochromatics

Unlike the Yoffe crack,[21] the near-field solution of eqs (1) and (2) shows that the dynamic stress-intensity factor will not approach that of the static stress-intensity factor, $K$, as $r = \sqrt{x^2 + y^2} \to 0$. The exact deviation between dynamic and static stress-intensity factors for a given crack velocity, $c$, varies with the procedure in which static near-field state of stress is fitted to the dynamic near-field state of stress. For example, if a two-parameter static isochromatic lobe is matched with a one-parameter dynamic isochromatic lobe at the maximum radial distance, $r_{max}$, as shown in Fig. 5, then the ratio of static to dynamic stress-intensity factors are 1.02 and 1.07 for $c/c_1 = 0.106$ and 0.159, respectively. Such inherent error in the estimation of dynamic stress-intensity factor is thus negligible at lower crack velocities of $c/c_1 < 0.1$ where much of the crack-arrest fracture toughness, $K_{Ia}$, is estimated. Otherwise, the above inherent error is unavoidable when a static near-field solution is used in place of a dynamic near-field solution regardless of the smallness of the region.

Having established the inherent error in the use of the static state of stress for dynamic-stress-intensity-factor estimation, we then posed the question of what additional errors, if any, are involved by evaluating the dynamic optical data in a larger region. For this purpose, the three-parameter representation of the dynamic near-field solution as shown by eq (1) was used to model a crack propagating at constant velocities of $c/c_1 = 0.00001$, 0.05 and 0.15. The dynamic state corresponding to $c/c_1 = 0.00001$ was used as the corresponding static solution after verifying the negligible discrepancy between the static and dynamic state of this extremely low crack velocity. Dynamic modulus $E = 4.65$ GPa (675 ksi) and Poisson's ratio $\nu = 0.345$ for Homalite-100 were used to simulate the actual test conditions in dynamic photoelasticity.

Typical dynamic states of $K/K_{IC} = 2$, and 0.8 surrounding the crack-tip propagating at the constant velocities of $c/c_1 = 0.15$ and 0.05, respectively, were considered, For comparison, isochromatic fringes which pass through a selected reference point* were plotted for $K/K_{IC} = 2.2$ and 1.8 in addition to the referenced $K/K_{IC} = 2.0$ at $c/c_1 = 0.15$ and 0.00001, as shown in Figs. 6 and 7. The smaller static isochromatic lobe of $c/c_1 = 0.00001$ in these figures indicates that an inherent overestimation of 24 percent in $K$ is involved if the static isochromatic lobe is only stretched to match $r_{max}$ of the dynamic isochromatic lobe in Fig. 6. Likewise, $K$ will be overestimated by 12 percent if the smaller dynamic isochromatics in Fig. 7 are considered. This increased error due to increased size in isochromatics indicates the importance of a dynamic

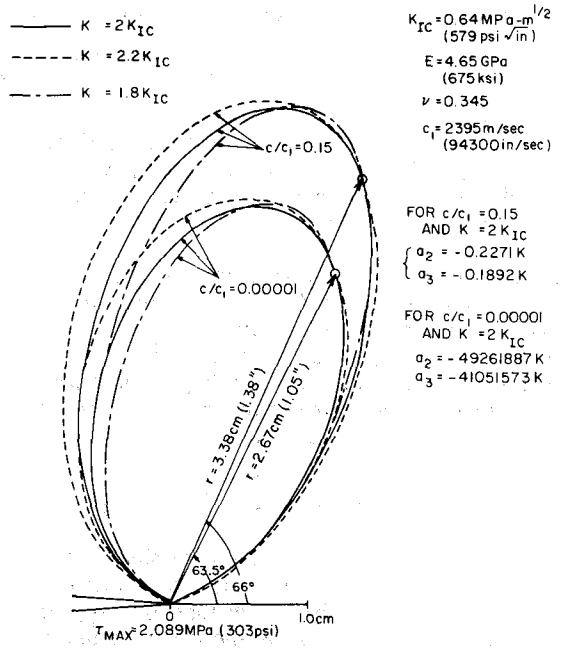


Fig. 6—Static and dynamic isochromatic lobes at a crack tip

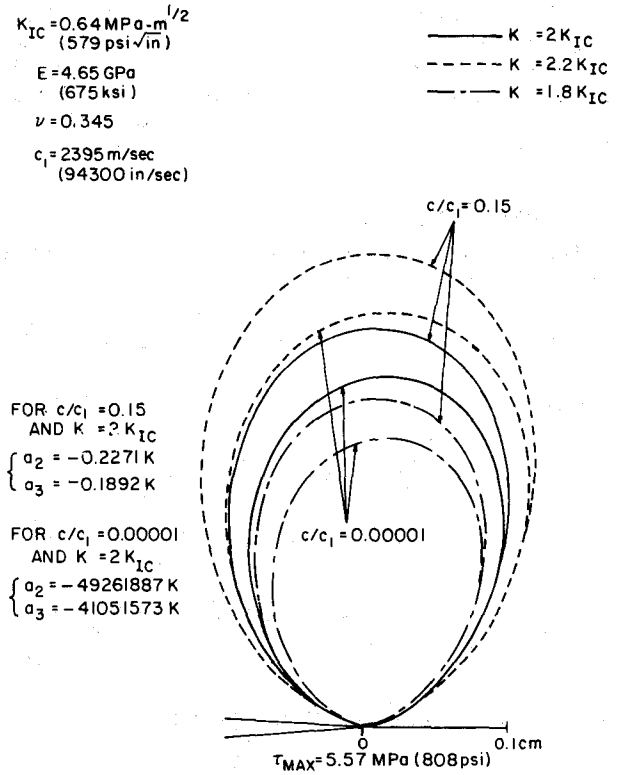


Fig. 7—Static and dynamic isochromatic lobes at a crack tip

* *These reference points were chosen to match the forward portion of the dynamic isochromatic lobes. These are not directly related to* $r_{max}$ *or* $\theta_{max}$.

analysis when larger isochromatic lobes are considered and is in qualitative agreement with the error analysis in Ref. 19 where the artificial Yoffe crack[21] was used to estimate the size effect in the backward tilting isochromatic lobes. Within a sufficiently close region surrounding the running crack tip and in the absence of any parasitic stress waves, the magnitude of this overestimation will be reduced, but the statically computed stress-intensity factor will always be larger than the actual dynamic value.

Figure 6 also indicates the relative insensitivity of the size of larger isochromatic lobe to a ±10 percent change in dynamic and static stress-intensity factors. Dimensional changes with small changes in stress-intensity factors are accomplished mainly by the small changes in the tilting of the isochromatic lobe, $\theta_{max}$, verifying the original conclusion by Bradley.[1] Such insensitivity to $K$ raises the possibility that the small oscillations in dynamic stress-intensity factor could be masked by the average dynamic stress-intensity factor of larger isochromatic lobes, unless the data-reduction procedure is sensitive to $\theta_{max}$ change.

The above numerical examples reconfirmed our suspicion that considerable error may be induced when the static near-field solution is used to compute the dynamic stress-intensity factor using relatively large isochromatics. The use of higher-order terms in the static eigen-function expansion formula to accommodate the larger isochromatics may not necessarily improve the accuracy in the data-reduction procedure but could increase the error involved at higher crack velocities.

Figure 8 shows the larger dynamic isochromatic lobes at crack velocities of $c/c_1 = 0.05$. Static isochromatic lobes were not included in Fig. 8 since these static isochromatics were at the most only 2-3 percent smaller in radial distances than the corresponding dynamic isochromatics. Likewise coincidence existed in the smaller isochromatics. Error analysis of our data-reduction procedure at this crack velocity is of particular interest since small differences in the dynamic stress-intensity factors, $K$, at this portion of the Γ-curve could result in different crack-arrest stress-intensity factor, $K_{Ia}$, which is often estimated by extrapolating the lower end of the Γ-curve at $c/c_1 = 0$. Figure 8 shows that, for slower crack velocities of $c/c_1 = 0.05$, the static near-field isochromatics is a reasonable representation of the dynamic state. Data scatter observed in the lower end of the Γ-curve in Figs. 2 and 4 could thus be due to either experimental errors or the actual fluctuations in $K$.

As another assessment of possible error involved in using larger isochromatic lobes, a constant-velocity crack of $c/c_1 = 0.15$ running into a constant and linearly varying static stress fields of $\sigma_{yy} = 0.689$ MPa (100 psi) at $y \neq 0$ and $0.689 \cdot y$ MPa ($100 \cdot y$ psi), respectively, were considered. Such stress fields simulate two types of reflected tension waves impacting the constant-velocity crack and represent the dynamic near-field solution immediately prior to the elevation in dynamic stress-intensity factor due to the impinging tensile waves. The magnitude as well as the gradient of these impinging tensile wavefronts were taken from the experimental values of transient waves in Ref. 25. Figures 9 and 10 show the two levels of near-field isochromatics with the superimposed $\sigma_{yy} = 0.689$ MPa (100 psi) and $0.689 \cdot y$ MPa ($100 \cdot y$ psi), respectively. Also shown in Figs. 9 and 10 are the dynamic near-field isochromatics without the superimposed static states of stress. It is immediately obvious that the larger dynamic isochromatics are significantly altered by the superimposed moderate tensile field. In terms of the data-reduction procedure, the larger isochromatics will predict a significantly higher apparent dynamic stress-intensity factor, while the smaller isochromatic lobes which are dominated by the dynamic singular stress field will predict more accurately the instantaneous dynamic stress-intensity factor.

### Dynamic Caustics

The dynamic near-field region considered by eq (5) relates to a region of $r_{max} \doteq 0.1$ in.[8] Thus, the inherent error as well as the possible error involved in predicting dynamic stress-intensity factors in the presence of an impinging stress wave follow those involved in the smaller isochromatic lobes discussed previously. The qualitative agreement in data scatter in Fig. 4 and the observed oscillation in dynamic stress-intensity factors could be explained by the similarity in Kalthoff's and our data-reduction procedures which are confined to the smaller near field surrounding the running crack.

## Conclusions

1. Qualitative agreements between the dynamic fracture toughness of Homalite-100 plates obtained by T. Kobayashi *et al.* and the wedge-loaded DCB results for Araldite B by Kalthoff *et al.* and the author's old results are observed.
2. Differences in the various results obtained by the three teams of investigators could be attributed, in part, to the accuracy and interpretation of crack-velocity data.
3. The use of static near-field stresses in place of the dynamic near-field stresses in computing the dynamic stress-intensity factors could result in overestimation of these values at the higher crack velocity of $c/c_1 = 0.15$.
4. An impinging stress wave on a moving crack could significantly change the shape of larger isochromatic lobes and thus introduce substantial error in the computed stress-intensity factor.
5. If the static stress field must be used in evaluating the dynamic photoelasticity results at higher crack velocities

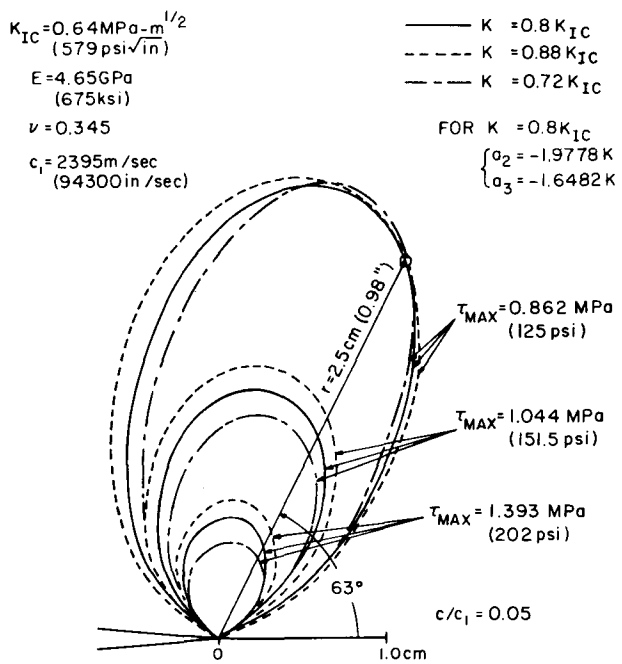

Fig. 8—Dynamic isochromatic lobes at a crack tip

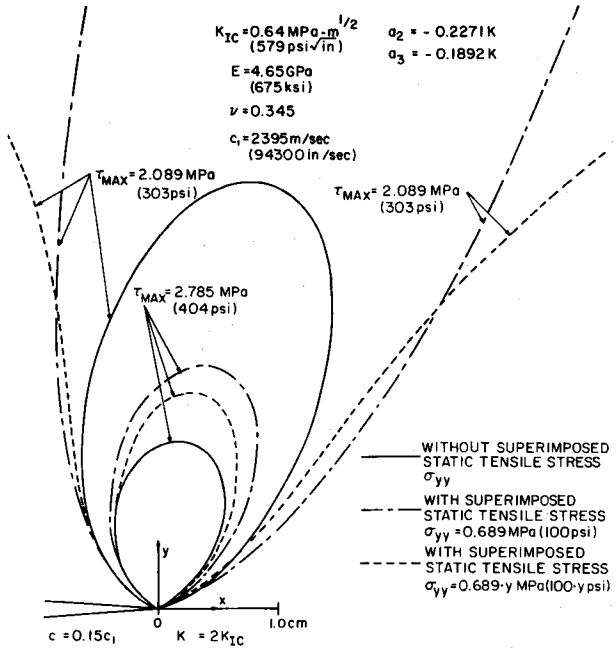


Fig. 9—Dynamic isochromatic lobes at a crack tip with superimposed static tensile stress, $\sigma_{yy}$

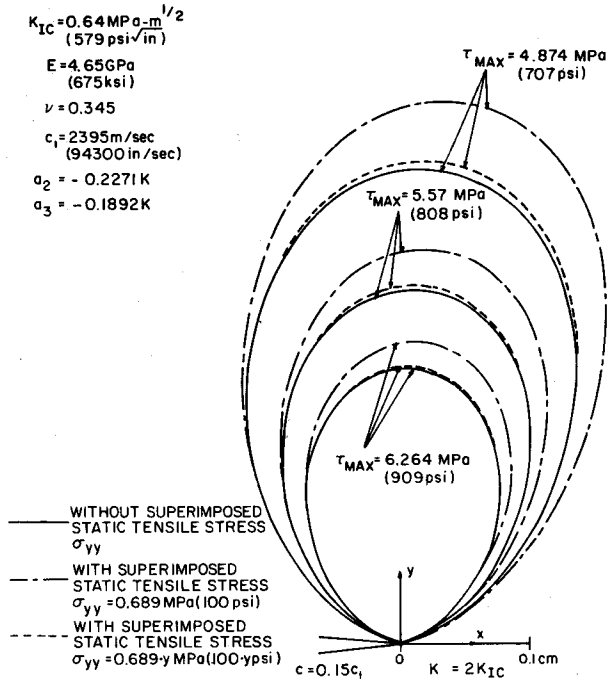


Fig. 10—Dynamic isochromatic lobes at a crack tip with superimposed static tensile stress, $\sigma_{yy}$

or in the presence of parasitic stress waves, the dynamic stress-intensity factors should be computed by using the smallest isochromatics, preferably within 2.5 mm (0.1 in.) distance of the crack tip at higher crack velocities.

## Acknowledgment

The results of this investigation were obtained in a research contract funded by the Office of Naval Research under Contract No. N000014-76-C-0060, NR 064-478. The authors wish to acknowledge the support and encouragement of Drs. N.R. Perrone and D. Mulville of ONR.

## References

*1. Kobayashi, A.S., Wade, B.G. and Bradley, W.B., "Fracture Dynamics of Homalite-100," Deformation and Fracture of High Polymers, H.H. Kausch, J.A. Hassell, and R.I. Jaffee, eds., Plenum Press, New York, 487-500 (1973).*

*2. Wade, B.G. and Kobayashi, A.S., "Photoelastic Investigation on the Crack-arrest Capability of Pretensioned Stiffened Panels,"* EXPERIMENTAL MECHANICS, **15** *(1), 1-9 (Jan. 1975).*

*3. Kobayashi, A.S. and Chan, C.F., "A Dynamic Photoelastic Analysis of Dynamic-tear-test Specimen,"* EXPERIMENTAL MECHANICS, **16** *(5), 176-181 (May 1976).*

*4. Kobayashi, A.S., Mall, S. and Lee, M.H., "Fracture Dynamics of Wedge-Loaded DCB Specimen," Cracks and Fracture, ASTM STP 601, 274-290 (1976).*

*5. Irwin, G.R., "Discussion and Authors' Closure of the Paper, 'The Dynamic Stress Distribution Surrounding a Running Crack—A Photoelastic Analysis'," Proc. SESA,* **XVI** *(1), 93-96 (1958).*

*6. Kobayashi, T. and Fourney, W.L., "Dynamic Photoelastic Investigations of Crack Propagation," Proc. 12th Annual Mtg. Soc. Engrg. Sci., Univ. Texas—Austin, 131-140 (Oct. 20-22, 1975).*

*7. Kobayashi, T. and Dally, J.W., "The Relation Between Crack Velocity and Stress Intensity Factor in Birefringent Polymers," Fast Fracture and Crack Arrest, ASTM STP 627, 257-273 (Jul. 1977).*

*8. Kalthoff, J.F., Beinert, J. and Winkler, S., "Dynamic Stress Intensity Factors for Arresting Cracks in DCB Specimens," Fast Fracture and Crack Arrest, ASTM STP 627, 161-176 (Jul. 1977).*

*9. Döll, W., "Investigation of the Crack Branching Energy," Int. J. Fract.,* **11**, *184-186 (1974).*

*10. Bergkvist, H., "Some Experiments on Crack Motion and Arrest in Polymethylmethacrylate," Engrg. Fract. Mech.,* **6**, *621-626 (1974).*

*11. Irwin, G.R., "Comments on Dynamic Fracture Testing," Proc. Int. Conf. Dynamic Fract. Toughness, Welding Inst., 1-9 (Jul. 1976).*

*12. Urabe, Y., Kobayashi, A.S., Emery, A.F. and Love, W.J., "Dynamic Finite Element Analysis of a Tapered DCB Specimen," to be published in Proc. Int. Conf. Fract. Mech. Tech., Hong Kong (Mar. 21-25, 1977).*

*13. Emery, A.F., Love, W.J. and Kobayashi, A.S., "Influence of Dynamic Fracture Toughness on Elastic Crack Propagation in a Pressurized Pipe," to be published in Proc. Int. Conf. Fract. Mech. Tech., Hong Kong (Mar. 21-25, 1977).*

*14. Kobayashi, A.S., Mall, S. and Bradley, W.B., "Dynamic Photoelastic Analysis of Crack Branching," Proc. 12th Annual Mtg. Soc. Engrg. Sci., Univ. Texas—Austin, 1005-1014 (Oct. 20-22, 1975).*

*15. Hahn, G.T., Gehlen, P.C., Hoagland, R.G., Kanninen, M.F., Popelar, C. and Rosenfield, A.R., "Critical Experiments, Measurements and Analyses to Establish a Crack Arrest Methodology for Nuclear Pressure Vessel Steels," 4th Quart. Prog. Report, Task 62, Battelle Columbus Labs, BMI-1939 (Nov. 1975).*

*16. Freund, L.B., "Crack Propagation in an Elastic Solid Subjected to General Loading-I, Constant Rate of Extension," J. Mech. Phys. Solids,* **20**, *129-140 (1972).*

*17. Nilsson, F., "A Note on the Stress Singularity at a Non-Uniformly Moving Crack Tip," J. Elasticity,* **4**, *73-75 (1974).*

*18. Kanninen, M.F., Mills, E., Hahn, G.T., Marschall, C.W., Borek, D., Cogle, A., Masubuchi, K. and Itoga, K., "A Study of Ship Hull Crack Arrester Systems," Battelle Columbus Labs Report, Contract N00024-75-C-4325 (Dec. 18, 1975).*

*19. Kobayashi, A.S., Emery, A.F. and Mall, S., "Dynamic Finite Element and Dynamic Photoelastic Analyses of Crack Arrest in Homalite-100 Plates," Fast Fracture and Crack Arrest, ASTM STP 627, 95-108 (1977).*

*20. Irwin, G.R., Dally, J.W., Kobayashi, T. and Etheridge, J.M., "A Photoelastic Study of the Dynamic Fracture Behavior of Homalite-100," NUREG-75/107, US NRC (Sept. 1975).*

*21. Yoffe, E.H., "The Moving Griffith Crack," Phil. Mag.,* **42**, *739-750 (1951).*

*22. King, W.W., Malluck, J.F., Aberson, J.A. and Anderson, J.M., "Application of Running Crack Eigenfunction to Finite Element Simulation of Crack Propagation," Mech. Res. Comm.,* **3** *(3), 197-202 (1976).*

*23. Williams, M.L., "On the Stress Distribution at the Base of a Stationary Crack," J. Appl. Mech., Trans. ASME,* **24** *(2), 109-114 (1957).*

*24. Theocaris, P.S., "Local Yielding Around a Crack Tip in Plexiglass," J. Appl. Mech., Trans. ASME,* **37**, *Series E (2), 409-415 (Jun. 1970).*

*25. Kobayashi, A.S. and Wade, B.G., "Crack Propagation and Arrest in Impacted Plates," Proc. Int. Conf. Dynamic Crack Propagation, G.C. Sih, ed., Noordhoff Int. Pub., Leyden, 663-677 (1974).*